# Characterization results from several commercial soft x-ray streak cameras

G. L. Stradling and J. K. Studebaker

Los Alamos National Laboratory, Physics Division
P-14, Mail Stop D410, Post Office Box 1663, Los Alamos, New Mexico 87545 USA

C. Cavailler, J. Launspach and J. Planes

Commissariat a l'Energie Atomique, Centre d'Etudes de Limeil-Valenton
B.P. no 27, 94190 Villeneuve-Saint-Georges, FRANCE

## Introduction

We are presenting test results which compare spatio-temporal resolution characteristics of three commercially manufactured soft x-ray streak cameras and a prototype of the C650X soft x-ray streak camera made at CEA Limeil-Valenton using an RTC P650X streak tube[1] and now commercially available from the Thomson CSF[2] company.

These tests have been performed using ultra short x-ray pulses both at the Forge[3] pulsed x-ray source facility at Los Alamos National Laboratory in the United States and at the Ketjak laser facility[4] at CEA Limeil-Valenton in France.

The purpose of this research is to evaluate the relative performance of the C650X, the Hadland[5] X-Chron 540, the Hamamatsu[6] C1936X and the low magnification Kentech[7] soft x-ray streak cameras. Experimenters in the ultra-high-speed community need this information to make knowledgeable choices of instrumentation for time resolved x-ray experiments in the subnanosecond and nanosecond range. Often experiments require many time resolved detection channels which are both contiguous and synchronous in a single measurement. Time resolved x-ray spectroscopy or x-ray imaging experiments which use streak cameras as ultra-high-speed position sensitive x-ray detectors are frequently constrained by limited information density.

Optimization of the experiments and quantitative understanding of the data require knowledge of both the contrast transfer function (CTF) in the spatial axis of the instrument during the streak and the temporal resolution. This is the spatio-temporal performance character of the instrument.

Complete studies of these dynamic performance features have not previously been done with these instruments. Particular care must be taken to measure performance under relevant conditions and to make complete measurement sets[8]. We have found that there can be significant differences in the static CTF and the CTF measured in the streaked mode. The CTF is not usually constant across the streaked image. These characteristics obviously vary between instruments.

This set of tests is directed toward the class of instruments which use a large electron extraction field at the photocathode in order to obtain temporal resolution limits of a few picoseconds at the fastest sweep speeds. Compared to low extraction field designs, this high extraction field configuration can result in degraded CTF for some streak tubes[9].

We have not performed detailed CTF characterizations on the two picosecond range x-ray streak cameras which use the RCA C73435 and the similar RTC P501 tubes. Our extensive experience with these instruments[9,10] has shown them to have limiting dynamic spatial resolutions which are considerably poorer than those discussed here when used with high extraction fields in the picosecond regime. This experience is corroborated by measurements of the LLNL soft x-ray streak cameras recently published by Glendinning and Medecki[11]. Their paper also presents performance measurements of the Kentech 2X magnification x-ray streak camera.

## The Soft X-ray Streak Cameras

For the purpose of an informed comparison, we have listed important features of the four instruments in Table 1. More complete descriptions may be obtained in the literature and from the manufacturers. We will try to include relevant observations on subjective operational differences as well as quantitative performance measurements. All of the instruments use avalanche transistor sweep drivers. All of the data have been obtained on Kodak negative film after the intensification of the streak tube signal by micro-channel plate image intensifiers (ITT type F4113, F4112). The Kentech and Hadland data were taken with Royal X Pan film. The C650X and Hamamatsu data were taken with type 2485 film.

Table 1. Soft x-ray streak camera features.

| | C650X | Hadland X-Chron 540 | Hamamatsu C1936 | Kentech |
|---|---|---|---|---|
| Streak tube Tube type | RTC P650 Bi-lamellar focus | Photochron II conventional | N2019 conventional | Kent low magnif. |
| Astigmatism correction | Yes | Yes Each Speed | Yes | No |
| Cathode voltage (kV) | -15 | -17.0 | -6.5 | -14.8 |
| Extraction field (kV/cm) | 60 | 20 | 7.5 | 20 |
| Photocathode to extraction grid space (mm) | 2.5 | 0.5 | 2.0 | 2.0 |
| Useful photo-cathode length (mm) | 12 | 17 | 10 | 25 |
| Photocathode slit width (microns) | 100 | 80 | 80 | 200 |
| Photocathode configuration | 2X15mm² area separate from slit | on slit | on slit | 5X30mm² area separate from slit |
| Tube magnification | 2X | 1.6X | 1.6X | 1.2X |
| Tube length (cm) | 40 | 30 | 15 | 34 |
| Sweep speeds (psec/mm) | 40<br>50<br>80 | 20 500<br>50 1000<br>100 2000<br>200 5000 | 66<br>133<br>333<br>666 | 12.5 83<br>28.6 250<br>50 1000 |
| Photocathode accessibility | requires instrument demounting for access* | remotely demountable for inspection and replacement | remotely demountable for inspection and replacement | requires instrument demounting for access |
| Phosphor screen size(mm) | 63 | 50 | 25 | 50 |
| Relative camera sensitivity | 0.1 | 1 | 1 | 1 |
| Image intensifier used | ITT F4113 40 mm | ITT F4113 40 mm | ITT F4112 25 mm | ITT F4113 40 mm |
| Vacuum pumping | small turbo pump | small turbo pump | 8 l/s ion pump | pumped by experiment vacuum system |
| Tube construction | glass, Kovar | ceramic, stainless steel epoxy casting | glass, Kovar | Aluminum plastic standoff Open to chamvacuum in reentrant design |

* Remote photocathode manipulation is available in new models.

C650X

This instrument has been designed for optimum spatio-temporal resolution. The concept of the bi-lamellar P650X (Figure 1) tube is based mainly on two technological advances. The first is an intense accelerating field applied to the photocathode (60kV/cm). The second is the use of two focusing electron lenses designed to work independently. A quadrupole lens is used for spatial focusing and a separate cylindrical electrostatic lens focuses in the temporal direction.

The C650X streak camera (Figure 2) is conveniently self contained with the control settings on the camera chassis; sweep window durations and differential variations of the sweep speed along the screen are supplied with the camera. The soft x-ray tube is actively vacuum pumped with a small 40 l/s turbo pump. The instrument slides away from the chamber on a rail for photocathode access and replacement. This operation can be performed several times a day if necessary. The photocathode slit is 12 mm. Thin film photocathodes (300 A gold on 3000 A parylene) have been used for these tests.

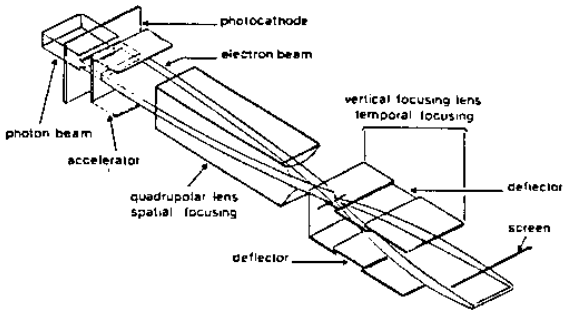


Fig. 1. The electron imaging configuration of the bi-lamellar P650X streak tube.

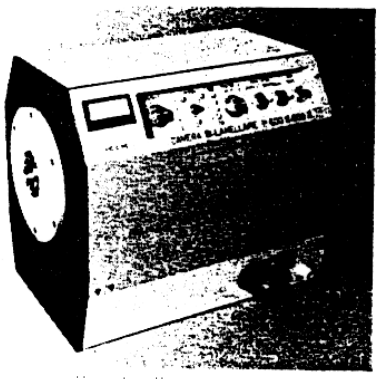

Fig. 2. The C650X soft x-ray streak camera. A new bi-lamellar electron imaging design is used in this instrument.

Hadland X-Chron 540

This instrument was engineered to meet a stringent Los Alamos specification. The design constraints focus on spatial resolution, on user convenience and on reliability and flexibility under laboratory conditions. This streak camera is compact in a single chassis (Figure 3). A wide variety of sweep speeds and sweep options are switch controllable at the chassis. Astigmatism focus corrections for the various sweep speeds are separately controlled. The photocathode can be extended remotely for viewing through a vacuum window without breaking vacuum. The photocathode can be replaced in less than 30 minutes by removing the vacuum window without moving the streak camera. The useable photocathode slit length is 17 mm. A 40 l/s turbo pump provides active vacuum pumping of the streak tube. A 4x5 cut film back is provided for image recording in addition to a Polaroid film back. A durable ceramic, stainless steel and cast epoxy streak tube construction is used.

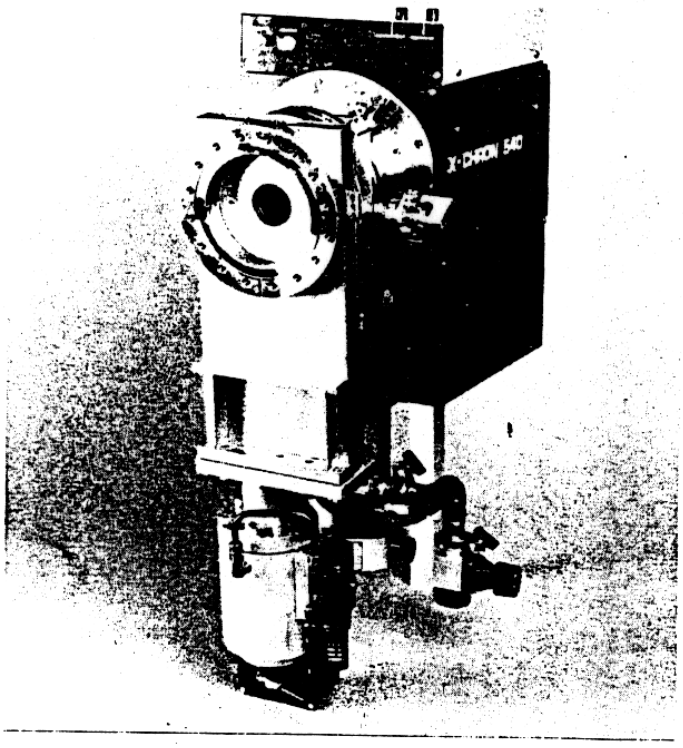


Fig. 3. The Hadland X-Chron 540 soft x-ray streak camera features a large photocathode which is remotely demountable.

Hamamatsu C1936

The Hamamatsu soft x-ray streak camera (Figure 4) was also engineered to meet the same Los Alamos specification as the Hadland X-Chron 540. The streak camera is also compact with all of the adjustments on the camera chassis. A small external power supply is part of the system. Four sweep speeds are used. The photocathode may be remotely extracted for external viewing through a vacuum window. Photocathode replacement is executed without moving the streak camera. An 8 l/s ion pump actively pumps the streak tube. Astigmatic focus correction is integrated into this streak camera. A 35 mm motor drive film back is available; however, a standard 4x5 Polaroid film back is not offered. The photocathode is relatively small, 10 mm.

Low Magnification Kentech

This instrument (Figure 5) was engineered for re-entrant positioning of the photocathode close to the x-ray source inside of the experimental chamber. It fits in a 10 inch port and extends 20 cm into the chamber. The streak tube of this model produces a 1.2X magnification. A 2X magnification model is also available. The sweep control chassis, the EHV power supply chassis and the user supplied intensifier controls and supplies are separate from the camera. The mechanical engineering is inferior to the other three instruments tested but appears to be adequate for many applications. The photocathode and cathode slit mask are supplied as separate items. A Polaroid film back is available but a negative film back is not offered. The streak tube, which resides in the experiment chamber and depends on the experiment vacuum system, is assembled of plastic and aluminum parts. The useable photocathode length is a relatively long 25 mm.

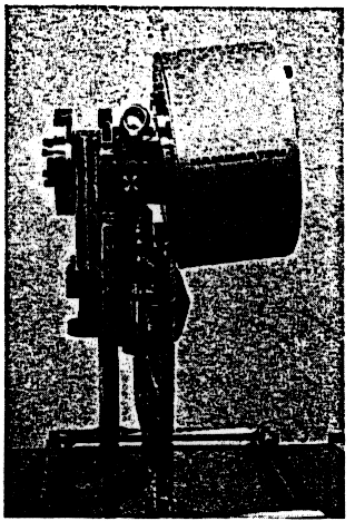

Fig. 4. The Hamamatsu C1936X soft x-ray streak camera features a remotely demountable photocathode.

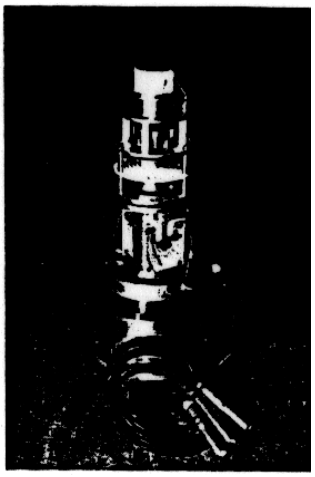

Fig. 5. The low magnification Kentech x-ray streak camera. This camera utilizes a re-entrant design and a 25 mm photocathode.

## Experimental facilities

### The Forge

The Forge pulsed x-ray source facility (Figure 6) at Los Alamos National Laboratory uses a high power ND:glass laser to focus 1.5 J of 1.06 micron light onto a 100 micron spot on a target in 100 psec. The laser pulsewidth can be varied up to 1 nanosecond. The Forge x-ray source is viewed by the streak cameras through a vacuum. An aluminized 50 microgram/cm$^2$ CH filter is used for these measurements as a UV and charged particle shield. The target to streak camera photocathode distance is 56 cm for the Hadland and Kentech cameras and 66 cm for the Hamamatsu camera.

The laser irradiation conditions in these measurements were held to 0.18 J at $2 \times 10^{13}$ W/cm$^2$ onto a gold slab target. Higher energy laser pulses resulted in saturation level exposures in the streak cameras.

The photocathodes on the Hadland, Hamamatsu and Kentech cameras consist of thin films [300 A Al on 1000 A parylene(CH)] which are directly mounted onto the cathode slit apertures of the streak tubes.

### The Ketjak Laser Facility

The Ketjak laser facility at CEA Limeil-Valenton uses a high-power ND:glass laser to focus 50 psec pulses of 1.06 micron light in a 100 micron spot onto a metallic target. Under these conditions the laser produced plasma delivers one or more x-ray pulses of approximately 50-70 psec duration. The C650X streak camera is coupled to the experiment vacuum chamber and views the target through an aluminized CH filter used as a UV and charged particle shield. The target to streak camera photocathode distance is 130 cm.

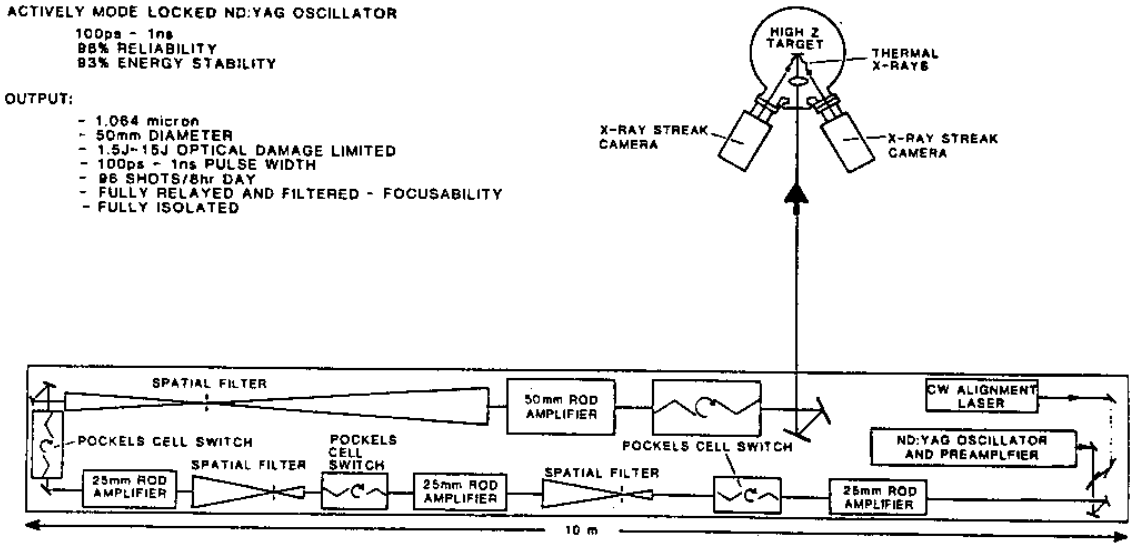


Fig. 6. The Forge pulsed x-ray source facility.

## Measurement Technique

Streak camera resolution in both the temporal and the spatial dimensions of the streak images are measured. We have observed that the temporal and spatial resolution characteristics of some earlier streak cameras are mutually dependent and that to optimize resolution in one axis requires a compromise in the resolution in the other axis. Thus both features must be evaluated under the same focus conditions.

### Spatial resolution

A variety of resolution masks were used to map out the contrast transfer character of the four instruments. In all cases, the resolution masks discussed in this comparison consist of free standing gold bars separated bay spaces nominally equal to the bar width. The 18 micron thick gold bars are completely opaque to the incident x-radiation. This produces total shadowing of the photocathode at the spatial frequency of the mask. We used shadow masks with spatial frequencies of 5, 8, 10, 12.5, 16, or 20 lp/mm.

The mask is positioned 1 to 2 mm from the photocathode (Figure7). Penumbral blurring of the shadow by the source size and by the experiment geometry is less than 0.2 micron and is negligible.

The spatial frequency values in this comparison refer to that of the shadow mask at the streak camera photocathode instead of that in the streak image. The various streak tubes have different values of photocathode-to-screen image magnification.

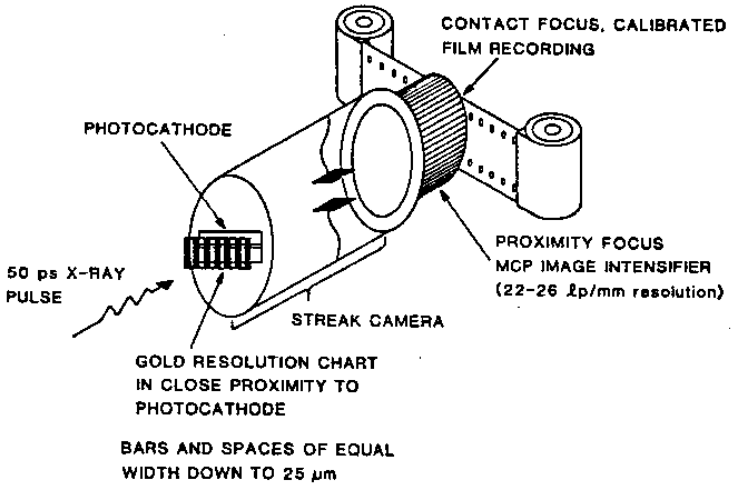


Fig. 7. A schematic representation of the contrast mask at the x-ray streak camera photocathode. The mask is positioned 1 to 2 mm from the photocathode.

Temporal resolution

X-ray pulses with pulse lengths less than the temporal resolution of these instruments were not readily available. In order to estimate the temporal resolution, we evaluate the imaging fidelity in the temporal direction and calculate the expected temporal response. Where the pulse shapes and energy distributions may be taken to be Gaussian, the temporal resolution is approximated[12] by the quadratic sum of the instrumental resolution tv and the transit time dispersion td:

$$t = (t_v^2 + t_d^2)\ 1/2$$

The minimum time resolved element, $t_v$, for a given sweep speed $V^{-1}$ (psec/mm) and the experimental (unswept) width, $x_s$, of the slit image in the temporal direction is given by:

$$t_v = x_s\ V^{-1}$$

The transit time dispersion $t_d$ resulting from the photo-electron energy spread, $\Delta e$ (eV), and field E(V/cm) on the photocathode is given by[12]:

$$t_d = 2.3 \times 10^{-8}\ \frac{(\Delta e)^{\frac{1}{2}}}{E}$$

The energy spread, $\Delta e$, of 6.5 eV or 4.6 eV for incident 1487eV x-ray photons on gold or aluminum respectively may be had from Henke[13].

Data Processing and Analysis

Film digitization

The data was recorded on negative film with a density calibration wedge. The image was then scanned with a microdensitometer at aperture sizes appropriate to the spatial frequency of the data in the image. The digitized data was then converted to relative intensity values through the density versus log exposure (D-vs-logE) calibration data.

Digitization of those data was performed with a Joyce-Loebl microdensitometer at CEA Limeil-Valenton and with a PDS computer controlled microdensitometer at Los Alamos. Image processing was accomplished using a Recognition concepts image processor.

Signal-to-noise ratio enhancement

High fidelity recording of temporal or spatial detail in an ultra-fast signal is limited by the signal-to-noise ratio in the image as well as by the streak system imaging capability. The signal-to-noise ratio becomes a more important issue as the recording time becomes shorter because the instantaneous charge current in the streak tube is limited by Coulomb repulsion effects. When this limit is exceeded, temporal and spatial fidelity of the system is degraded and saturation becomes apparent. Thus the integrated electron signal through the streak tube, Q, which must make up the streak image, is limited by the product of the tube saturation current and the signal pulse width.

$$Q < I_{max} * \Delta t$$

The image may be intensified to obtain adequate signal levels for film recording but this does not improve the shot-noise-limited statistical character of the data. Because of this signal level limitation, the full temporal and spatial fidelity of the streak system may not both be simultaneously available.

When we wish to analyze the streak image with emphasis on spatial fidelity, we may need to integrate signal in the temporal direction for a number of resolution times, t, to obtain adequate statistics for the full spatial resolution of the streak tube to be apparent. Similarly, if we wish to obtain the limiting temporal resolution of the instrument, it may be necessary to sum over a number of spatial resolution lengths for adequate statistical character in the temporal profile.

Spatial fidelity

Often the spatial resolution of a streak camera is specified in terms of that spatial frequency for which the contrast is at the limit of visual discernability. This "limiting spatial frequency" is an inadequate descriptor of instrument imaging fidelity for applications which require quantitative image analysis. A more quantitative measure of instrument performance is the contrast transfer function (CTF).

The contrast modulation in the data is defined here as the ratio of the intensity modulation to the peak intensity with an adjustment for the background level of the film.

$$\text{Contrast} = \frac{L_{max} - L_{min}}{L_{max} - \text{background}}$$

The parameters $L_{max}$, $L_{min}$, and the background level are illustrated in Figure 8. The contrast was observed to vary with position in the streak image. In these characterization tests, we have used flux levels as high as possible without going into saturation. However, it has been necessary to use the integration techniques described above to evaluate the full temporal and spatial capabilities of the instruments. Substantial signal averaging in the temporal direction was necessary to reduce the error in contrast level to the few percent level. The uncertainty in contrast as well as the integration time used in each measurement is listed with that value in Table 2.

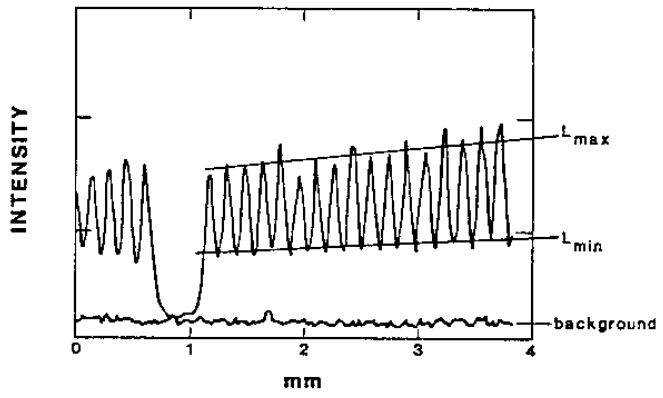


Fig. 8. Typical intensity versus position data from a contrast chart image. The parameters $L_{max}$, $L_{min}$, and the background level used to define the contrast value are labeled.

The system CTF as defined for our measurements corresponds to the image contrast at the output of the image intensifier and is plotted with respect to the spatial frequency of the shadow mask at the photocathode. Thus the CTF of the streak tube and the CTF of the image intensifier are combined to produce this system CTF. The different image magnification factors in the four streak tubes result in a given spatial frequency, measured at the photocathode, being transmitted through the image intensifier at different levels of contrast fidelity, depending on the actual spatial frequency at the image intensifier photocathode. While system CTF measurements provide a useful measure of system performance for practical applications, the effect of streak tube magnification and image intensifier CTF contribution to the system CTF should be considered when comparing the streak tube performances.

## Characterization results

Sample streak data from each of the four instruments is presented and analyzed in Figures 9 through 11. In Figure 9, typical streak images taken with a 10 lp/mm shadow mask are shown. Intensity versus position graphs from these images are shown in Figure 10. The nature of the noise induced contrast uncertainty is apparent here. The contrast values corresponding to a range of spatial frequencies are plotted as CTF curves for the four systems in Figure 11. Details of the various measurements are given below.

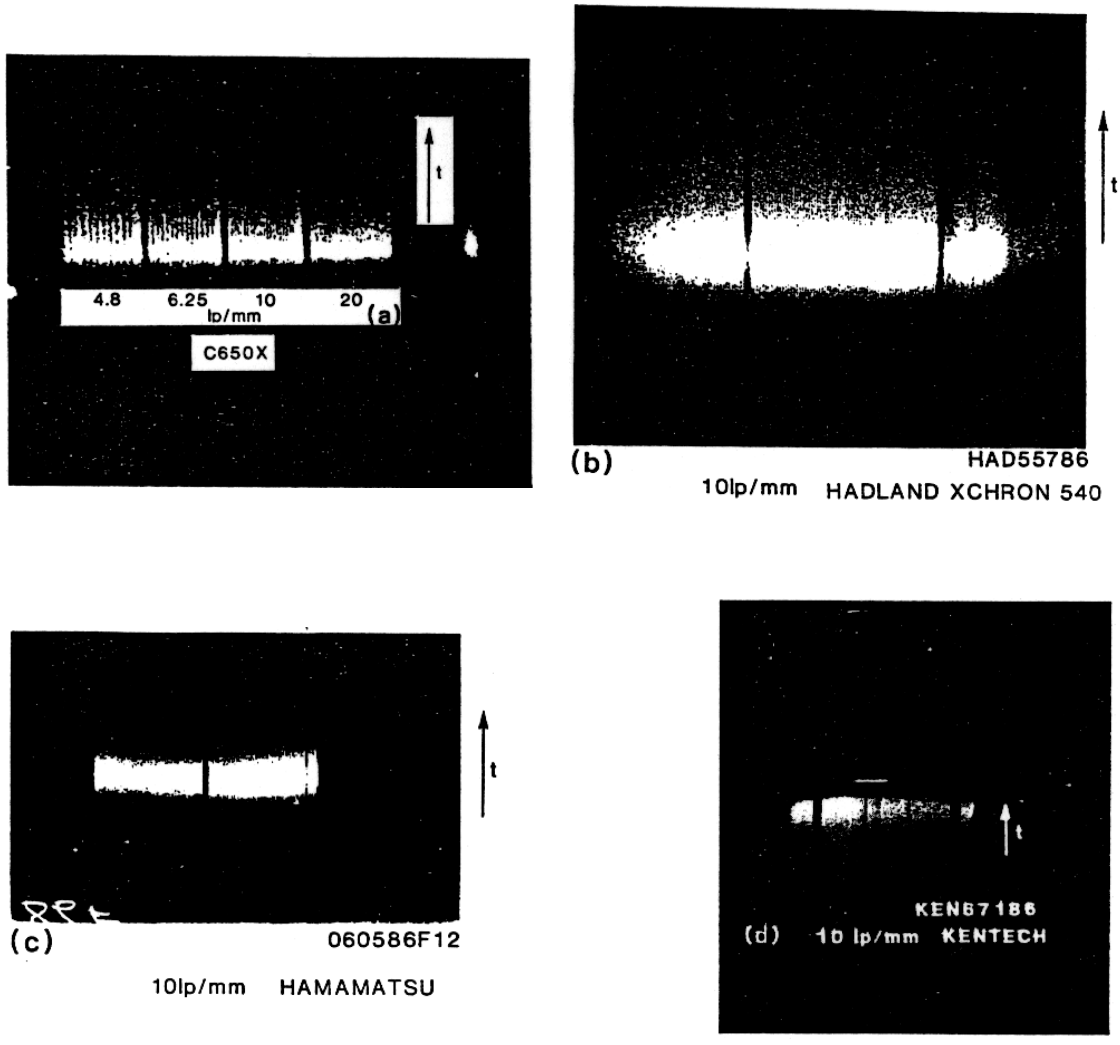


Fig. 9. Typical streak images taken with a 10 lp/mm shadow mask from each of the four instruments.

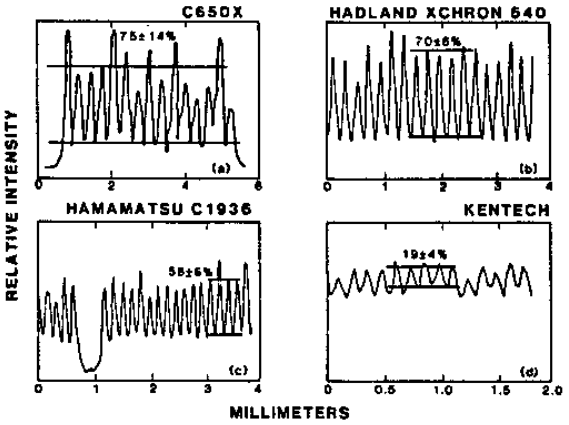


Fig. 10. Intensity versus position data from the four images of Fig. 9. The images were averaged 50 psec in the time direction to obtain contrast values with the level of consistency shown. The Hamamatsu data was only averaged 33 psec.

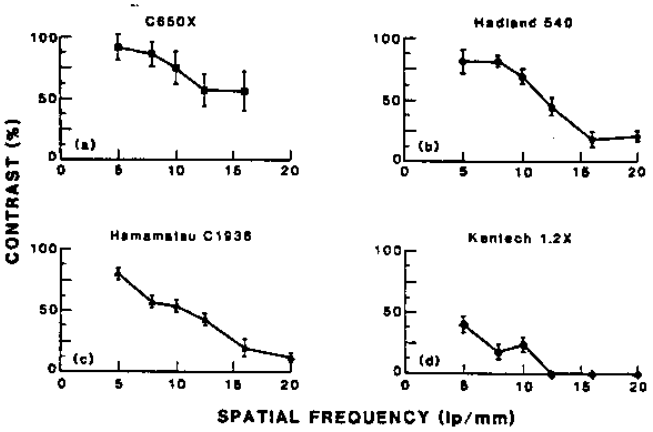


Fig. 11. Contrast transfer functions of the four x-ray streak cameras with the statistical uncertainty of the contrast values indicated.

C650X

The measurements on this instrument used the 50 psec x-ray pulse from the Ketjak facility. The unswept mode image of the lit produced with this x-ray pulse has an average width, $x_s$ in the temporal dimension, of 100 microns anywhere across the screen. With the sweep rate of $V^{-1}$ of 50 psec/mm, used in the dynamic measurements, we would obtain a temporal resolution value, t, of 4.1 psec anywhere on the screen.

At this sweep speed the dynamic temporal resolution extends to 20 lp/mm at the limit of visually discernable contrast. Signal averaging of 50 psec in the time direction was used determine the contrast at the 5, 8, 10, 12.5 and 16 lp/mm spatial frequency values respectively. The streaked image of a 10 lp/mm resolution chart is shown in Figure 9a. A plot of signal amplitude versus position for the 10 lp/mm data is given in Figure 10a. The contrast at 10 lp/mm is 85%. The contrast transfer function is given in Figure 11a.

This instrument has demonstrated uniform high fidelity recording capability across both spatial and temporal dimensions of the sweep. This advantage must be weighed against the tube throughput which is a factor of 10X lower in this streak camera than for the RCA 73435 tube based x-ray streak cameras.

Hadland X-Chron 540

The measurements presented for this instrument were performed with 150 psec duration x-ray pulses at the Forge x-ray source. The unswept mode image of the slit produced with this x-ray pulse has an average width, $x_s$, in the temporal dimension, of 170 microns at the screen center. At midpoint between the screen center and the end of the sweep the width of the static image degrades to 220 microns. With the sweep rate of $V^{-1}$ of 50 psec/mm, used in the dynamic measurements, we obtain a temporal resolution value, t, of 8.9 psec at the center of the screen.

At this sweep speed the dynamic temporal resolution extends to 20 lp/mm. Signal averaging of 50, 50, 50, 100, 50, and 50 psec in the time direction was necessary to unambiguously determine the contrast at the 5, 8, 10, 12.5, 16 and 20 lp/mm spatial frequency values respectively. The streaked image of a 10 lp/mm resolution chart is shown in Figure 9b. A plot of signal amplitude versus position for the 10 lp/mm data is given in Figure 10b. The contrast at 10 lp/mm is 79%. This contrast degrades to 59% at the edge of the screen. The contrast transfer function is given in Figure 11b.

Hamamatsu C1936

The measurements presented for this instrument were performed with 150 psec duration x-ray pulses at the Forge x-ray source. The unswept mode image of the slit produced with this x-ray pulse has an average width, $X_s$, in the temporal dimension, of 130 microns at the screen center. At midpoint between the screen center and the end of the sweep the width of the static image degrades to 190 microns. With the sweep rate of $V^{-1}$ of 66 psec/mm, used in the dynamic measurements, we obtain a temporal resolution value, t, of 10.9 psec at the center of the screen.

At this sweep speed, the dynamic temporal resolution extends to 20 lp/mm. Signal averaging of 15, 15, 33, 66, 100, and 130 psec in the time direction was necessary to unambiguously determine the contrast at the 5, 8, 10, 12.5, 16, and 20 lp/mm spatial frequency values respectively. The streaked image of a 10 lp/mm resolution chart is shown in Figure 9c. A plot of signal amplitude versus position for the 10 lp/mm data is given in Figure 10c. The contrast at 10 lp/mm is 54%. This contrast degrades to 34% at the edge of the screen. The contrast transfer function is given in Figure 11c.

Kentech

The measurements presented for this instrument were performed with 150 psec duration x-ray pulses at the Forge x-ray source. The unswept mode image of the slit produced with this x-ray pulse has an average width, $X_s$ in the temporal dimension, of 215 microns at the screen center. At midpoint between the screen center and the end of the sweep the width of the static image improves to 200 microns. With the sweep rate of $V^{-1}$ of 50 psec/mm, used in the dynamic measurements, we obtain a temporal resolution value, t, of 11 psec at the center of the screen.

At this sweep speed the dynamic temporal resolution extends to 10 lp/mm. Signal averaging of 15, 25 and 50 psec in the time direction was necessary to unambiguously determine the contrast at the 5, 8 and 10 lp/mm spatial frequency values respectively. The streaked image of a 10 lp/mm resolution chart is shown in Figure 9d. A plot of signal amplitude versus position for the 10 lp/mm data is given in Figure 10d. The contrast at 10 lp/mm is 24%. This contrast degrades to 10% at the edge of the screen. The contrast transfer function is given in Figure 11d.

## Summary of results

A comparison plot of the contrast transfer functions of the four soft x-ray streak camera is presented in Figure 12. The contrast results are summarized in Table 2.

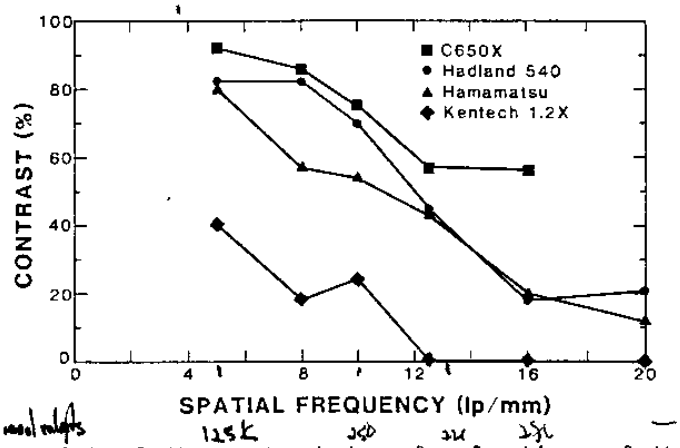


Fig. 12. A comparison plot of the contrast transfer functions of the four soft x-ray streak cameras.

TABLE 2 - Contrast results averaged over time for unambiguous determination of streak camera capability. The integration time is given in brackets[] . Edge of screen contrast values at the 10 lp/mm spatial frequency are given in parenthesis ().

| Spatial Frequency | C650X | Hadland X-Chron 540 | Hamamatsu C1936 | Kentech low mag. |
|---|---|---|---|---|
| 5 lp/mm | 92 ± 11% [50 psec] | 82 ± 10% [50 psec] | 80 ± 5% [15 psec] | 40 ± 7% [15 psec] |
| 8 lp/mm | 86 ± 10% [50 psec] | 82 ± 5% [50 psec] | 57 ± 5% [15 psec] | 18 ± 6% [25 psec] |
| 10 lp/mm | 75 ± 14% (75%) [50 psec] | 70 ± 6% (59%) [50 psec] | 54 ± 5% (34%) [33 psec] | 24 ± 6%(10%) [50 psec] |
| 12.5 lp/mm | 57 ± 13% [50 psec] | 45 ± 7% [50 psec] | 43 ± 5% [66 psec] | - - |
| 16 lp/mm | 56 ± 16% [50 psec] | 18 ± 6% [100 psec] | 20 ± 7% [100 psec] | - - |
| 20 lp/mm | | 21 ± 4% [50 psec] | 12 ± 4% [130 psec] | - - |

The effective temporal resolutions of the four instruments, at the fastest sweep speed available with the individual instruments, are tabulated in Table 3. The effective slit resolution in the temporal direction, X, coupled with the useful photocathode size, Lpc, the output screen size, D, and the spatial resolution at 40% contrast, R, results in a quantity: the information capacity of the streak system. Calculation of this quantity is slightly complicated by pragmatic constraints. The contrast transfer function may not be uniform across the image in space or in time. The entire 50mm screen on the large format streak tubes cannot be used with a 40mm diameter image intensifier. Thus, we use average values to compute the information capacity of the streak system which is taken to include a standard image intensifier size. In addition to the imaging limits of the streak system, statistical noise will constrain the achievable information capacity to well below this optimum value.

$$\text{Information capacity} = (2R_{ave} * L_{pc}) * (D_{II}/x_{ave})$$

Table 3 - Summary of optimized resolution and information capacity results.

| | C650X | Hadland X-Chron 540 | Hamamatsu C1936X | Kentech low mag. |
|---|---|---|---|---|
| $\tau_d$ | .97 psec | 2.5 psec | 6.7 psec | 2.5 psec |
| Fastest Sweep Speed | 40 psec/mm | 20 psec/mm | 66 psec/mm | 12.5 psec/mm |
| Average Static Slit Image Width $X_{ave}$ | 100 microns | 195 microns | 160 microns | 182 microns |
| $\tau_x$ | 4.0 psec | 3.9 psec | 10.6 psec | 2.3 psec |
| Average Temporal Resolution | 4.1 psec | 4.6 psec | 12.5 psec | 3.4 psec |
| Sweep Length w/II $O_{II}$ | 40 mm | 40 mm | 25 mm | 40 mm |
| Temporal Window at fastest sweep | 1.6 psec | 0.8 psec | 1.6 psec | 0.5 psec |
| Average Resolution at 40% $R_{ave}$ | 17 lp/mm | 10 lp/mm | 7.5 lp/mm | 2.1 lp/mm |
| Useful PC Length $L_{pc}$ | 12 mm | 17 mm | 10 mm | 25 mm |
| Information Capacity | 16 x $10^4$ pixels | 7.0 x $10^4$ pixels | 2.3 x $10^4$ pixels | 2.3 x $10^4$ pixels |

## Conclusions

The four soft x-ray streak cameras evaluated have shown good spatio-temporal fidelity. Each instrument was shown to have both strengths and weaknesses. The C650X has particularly high fidelity and uniformity of spatio-temporal resolution across the output screen. Users must weigh the relative advantages to their applications of spatial and temporal resolution, of resolution uniformity, photocathode length, user convenience and instrument cost.

It is important that shot noise degradation of the signal-to-noise ratio in the streak image be taken into account in experiment design and data analysis.

## Acknowledgments

We appreciate the extensive support of our management and technical staff both at Los Alamos and at CEA Limeil-Valenton. We particularly thank Dr.s Robert Day, Jacques Coutant and Alain Coudeville for their funding and encouragement through the span of this two year project. We appreciate the flexibility and responsiveness of Jack Clifford in film processing, Becky Gomez-Lujan in image digitization and George Jordan in software development.

## References

1. B. Boutry, C. Cavailler and N. Fleurot, "P600/650 X-ray streak camera with optimized spatio-temporal resolution", Proceedings 15th International Congress on High Speed Photography and Photonics, SPIE Vol. 348, p. 766, San Diego, 1982.

2. Thomson-CSF, Department Applications Speciales de l'Instrumentation, Division des Equipements Avioniques, 23 a 27, rue Pierre-Valette, 92242 Malakoff Cedex, France.

3. Stradling, T. R. Hurry, E. R. Denbow, M. M. Selph and F. P. Ameduri, "The Forge: a short pulse x-ray diagnostic development facility", Proceedings, Conference on High Speed Photography, Videography and Photonics, SPIE Vol. 569, 1985.

4. C. Cavailler, N. Fleurot, J. Launspach, R. Sauneuf and R. Verrecchia, "Soft x-ray P550 streak camera: characteristics and applications", Proceedings 15th International Congress on High Speed Photography and Photonics, SPIE Vol. 348, p. 760 (San Diego 1982)

5. Hadland Photonics Limited, Newhouse Laboratories, Newhouse road, Bovingdon, Hemel Hempstead, Herts. HP3 0EL U.K.

6. Hamamatsu Photonics K. K., 1126-1, Ichino-Cho, Hamamatsu City, Japan.

7. Kentech Instruments Ltd., Blackett Lab., Prince Consort Rd., London SW7 2BZ, U.K.

8. N. Fleurot, G. L. Stradling, "Characterization of streak camera systems," Proceedings 16th International Conference on High Speed Photography and Photonics, SPIE Vol. 491, p. 374, Strasborg, 1984; G. L. Stradling, "Workshop on standards for photonic streak camera characterization, "Proceedings-Conference on High Speed Photography, Videography and Photonics, SPIE Vol. 569, p. 136, San Diego, 1985.

9. E. D. Savoye, R. W. Engstrom and H. S. Zimmerman, "Design and Performance of a Charge Coupled Device (CCD) Streak Cameras", Proceedings-Conference on Recent Advances in TV Sensors and Systems, SPIE Vol. 203, p. 59, San Diego, 1979.

10. G. L. Stradling, D. T. Attwood and R. L. Kauffman, "A Soft X-ray Streak Camera", IEEE Journal of Quantum Electronics, Vol. QE-19, p. 604 (1983).

11. S. G. Glendinning and H. Medecki, "Resolution characteristics of Lawrence Livermore National Laboratory soft x-ray streak cameras", Rev. Sci. Instrum., Vol. 57, p. 2184, 1986.

12. B. Boutry and N. Fleurot, "X-Ray Streak Camera P600 with Optimized Spatial, Time Resolution", Proceedings- 14th International Congress on High Speed Photography and Photonics, p. 147, Moscow, 1980. A more detailed treatment of transit time dispersion, which requires some details of the electron optic geometry of the streak tube in addition to the values of the various potentials, is given by G. G. Gregory, S. A. Letzring, M. C. Richardson and C. D. Kiikka, "High timespace resolved photography of laser imploded fusion targets," Proceedings Conference on High Speed Photography, Videography and Photonics, SPIE Vol. 569 p. 141, San Diego, 1985. The derivation of which has been submitted by P. A. Jaanimagi and B. L. Henke to Rev. Sci. Instruments.

13. B. L. Henke, J. A. Smith and D. T. Attwood, "0.1-10-keV X-ray-induced electron emission from solids-models and secondary electron measurements," J. Appl. Phys., Vol. 48, p. 1852, 1977. These values, which are for the secondary electron energy spread of ion-cleaned photocathodes, are conservative. This reference shows that photocathodes of both metals which have not been ion cleaned, as ours have not, have significantly narrower energy distributions.